OPTICAL REVIEW Vol. 10, No. 1 (2003) 8–12

Volume Phase Transmission Gratings and Compact Configurations for Coarse Wavelength Division Multiplexing and Demultiplexing

W. H. HUANG, Y. AMITAI and A. A. FRIESEM

Department of Physics of Complex Systems, Weizmann Institute of Science, Rehovot 76100, Israel

(Received August 5, 2002; Accepted October 30, 2002)

Volume phase transmission gratings, that have high and uniform diffraction efficiency regardless of polarization of the incident light over a broad wavelength range, have been designed and recorded. Such gratings were incorporated successfully into a novel compact configuration of a coarse wavelength division demultiplexer. Calculated and experimental results of such gratings, and a compact four-channel demultiplexer operating in the 1500 nm to 1600 nm range are presented.

Key words: volume phase transmission grating; compact configuration; coarse wavelength division multiplexing and demultiplexing (CWDM and CWDDM)

1. Introduction

Coarse wavelength division multiplexing and demultiplexing (CWDM and CWDDM) technology can be exploited to increase the transmission capacity in short haul optical communication, such as metro-core and access networks.[1–3] This is achieved by simultaneously transmitting a number of wavelength channels through a single optical fiber. A key interface component in such CWDM and CWDDM networks is a device that either combines a number of different wavelength channels into one composite channel, (multiplexer), or divides a composite multiwavelength channel into separate single wavelength channels, (demultiplexer). These are typically designed to have widely separated wavelength channels with typical channel spacing of 20 nm in the range from 1500 nm to 1600 nm.[3]

The current technologies for such multi/demultiplexers can be broadly divided into two types: thin-film filter technology and grating-based technology. In the more widespread thin-film filter technology, discrete and separate thin-film filters are designed to have the cut-off characteristics to obtain a desired spectral profile for each wavelength channel.[4] On the other hand, grating-based multi/demultiplexers provide a more cost-effective solution for multi/demultiplexers in CWDM and CWDDM because the multiplexing or demultiplexing is achieved mainly with only one diffraction grating, simultaneously for a number of wavelength channels. Most compact grating-based multi/demultiplexers use a substrate-mode grating pair,[5–7] and cannot satisfy all the important requirements for having high and uniform channel efficiency, wide wavelength channel separation, and polarization independence.

In this paper, we propose specially designed volume phase transmission gratings and a novel compact configuration. Such gratings, when incorporated into the novel configuration, can satisfy simutaneously all the requirements desired from multi/demultiplexers in CWDM and CWDDM applications.

2. Geometrical and Optical Parameters of Volume Phase Transmission Gratings for CWDM and CWDDM

In this section we consider the basic relations of volume phase transmission gratings, and determine the needed geometrical and optical parameters so that they can be incorporated into CWDM and CWDDM applications. We start with Fig. 1 which schematically shows a section of a volume phase transmission grating, and the geometry of the incident and diffracted beams. We assume that the material in both sides of the grating has the same refractive index n as the average refractive index of the grating, d is the grating thickness, and θ_1 and θ_2 are the incident angle and diffracted angle, respectively.

From the coupled wave theory,[8–10] the diffraction efficiencies of a volume phase transmission grating, $\eta_\perp$ for TE polarization and $\eta_\shortparallel$ for TM polarization, are

$$\eta_\perp = \frac{\sin^2\sqrt{\nu_\perp^2 + \xi^2}}{1 + \dfrac{\xi^2}{\nu_\perp^2}},$$

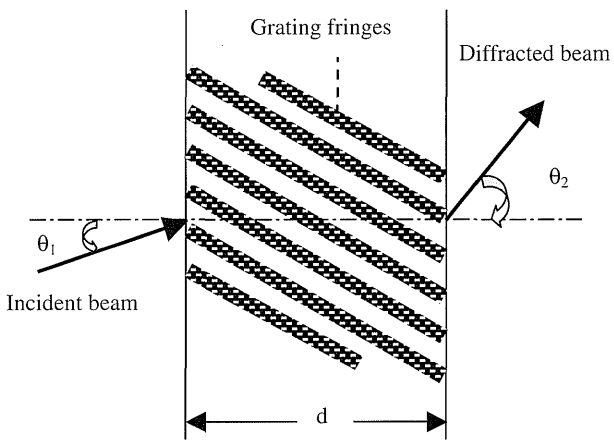

Fig. 1. Schematic illustration of a volume phase grating and geometry of the incident and diffracted beams. The grating thickness is d, the incident angle θ_1 and diffracted angle θ_2, respectively.

$$\eta_{\mathrm{II}} = \frac{\sin^2\sqrt{\nu_{\mathrm{II}}^2 + \xi^2}}{1 + \frac{\xi^2}{\nu_{\mathrm{II}}^2}}, \tag{1}$$

where

$$\begin{aligned} \nu_{\perp} &= \frac{\pi \cdot \Delta n \cdot d}{\lambda \cdot \sqrt{\cos(\theta_1) \cdot Cs}}, \\ \nu_{\mathrm{II}} &= \frac{\pi \cdot \Delta n \cdot d}{\lambda \cdot \sqrt{\cos(\theta_1) \cdot Cs}} \cdot \cos(\theta_2 - \theta_1), \\ \xi &= -\frac{(\lambda - \lambda_0) \cdot d \cdot K^2}{8\pi \cdot n \cdot Cs}, \\ Cs &= \cos(\theta_1) - K \cdot \cos\left(\frac{\theta_{01} + \theta_{02}}{2}\right) \cdot \frac{\lambda}{2\pi \cdot n}, \end{aligned} \tag{2}$$

and Δn is the refractive index modulation, λ is the illumination wavelength, θ_{01} and θ_{02} are the incident angle and diffracted angle at the Bragg wavelength λ_0, and K is the amplitude of the grating vector. According to Eqs. (1) and (2), the dependence of the diffraction efficiency on the polarization of the incident illumination can be relaxed by resorting to small $\Delta\theta = \theta_2 - \theta_1$. Specifically, when $\Delta\theta$ is small, the value of ν_{II} approaches that of $\nu_{\perp}$ so the value of $\eta_{\perp}$ approaches that of η_{Π}. Figure 2 shows the calculated diffraction efficiencies as functions of wavelength for both TE and TM polarizations, for four gratings with the same parameters of $d = 76\,\mu\mathrm{m}$, $\lambda_0 = 1550\,\mathrm{nm}$, $n = 1.44$, and $\Delta n = 0.005$, but different $\Delta\theta$ of (a) $\Delta\theta = 75°$, (b) $\Delta\theta = 45°$, (c) and (d) $\Delta\theta = 15°$. For these calculations we let $\theta_1 = \theta_{01}$ and $\Delta\theta \approx \theta_{02} - \theta_{01}$, since λ is not far from λ_0. As evident, the polarization dependence is strongest when $\Delta\theta = 75°$, and decreases as $\Delta\theta$ is reduced, becoming negligible when $\Delta\theta = 15°$. Additionally, the incident angle or diffracted angle does not greatly affect the polarization dependence as long as $\Delta\theta$ remains the same, as indicated in Eqs. (1) and (2), and in Figs. 2(c) and 2(d). It should be noted that for thick gratings, the wavelength discrimination becomes strong, as indicated in Fig. 2(a). This, of course, adversely affects the performance of the grating as a dispersion element. Fortunately, by letting $\Delta\theta$ be small, not only the polarization dependence but also the wavelength discrimination can be relaxed, as shown in Figs. 2(c) and 2(d).

Also, according to Eqs. (1) and (2), the diffraction efficiency increases as the refractive index modulation Δn and the grating thickness d increase, and decreases as the wavelength of illuminating light λ increases when the Bragg condition is satisfied, i.e. when $\xi = 0$. In practice, the recording materials usually have limited refractive index modulation of about $\Delta n = 0.015$ for visible wavelengths and even less for near infra-red wavelengths.[11,12] Thus, it is necessary to choose a sufficiently thick recording material so that high diffraction efficiency can be obtained for the limited refractive index modulation, especially when the illumination wavelength is relatively long. Figure 3 shows the calculated diffraction efficiencies as functions of wavelength for both TE and TM polarizations, for four gratings with the same parameters of $d = 76\,\mu\mathrm{m}$, $\lambda_0 = 1550\,\mathrm{nm}$, $n = 1.44$ and $\theta_{01} = 25°$, $\theta_{02} = 40°$, but different Δn of (a) $\Delta n = 0.002$; (b) $\Delta n = 0.005$; (c) $\Delta n = 0.007$; (d) $\Delta n = 0.008$. As evident, the diffraction efficiency increases significantly with refractive index modulation Δn, reaching almost 100% when $\Delta n = 0.008$. This value of Δn is readily available with photopolymer recording materials.

In general, volume phase transmission gratings can provide high and relatively uniform diffraction efficiency as a function of wavelength with negligible polarization dependence in a relatively broad wavelength range. This is

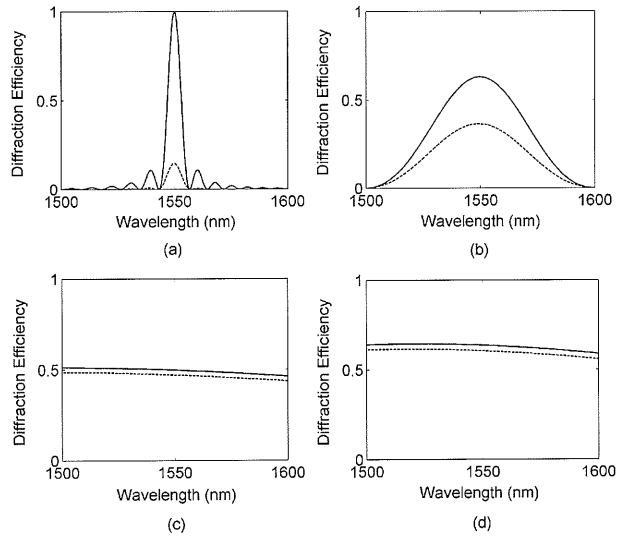

Fig. 2. Calculated diffraction efficiencies as functions of wavelength of volume phase transmission gratings for both TE (solid line) and TM (dotted line) polarizations. (a) $\theta_1 = 0°$, $\theta_2 = 75°$; (b) $\theta_1 = 0°$, $\theta_2 = 45°$; (c) $\theta_1 = 0°$, $\theta_2 = 15°$; (d) $\theta_1 = 25°$, $\theta_2 = 40°$. The four gratings have the same parameters of $d = 76\,\mu\mathrm{m}$, $\lambda_0 = 1550\,\mathrm{nm}$, $n = 1.44$ and $\Delta n = 0.005$.

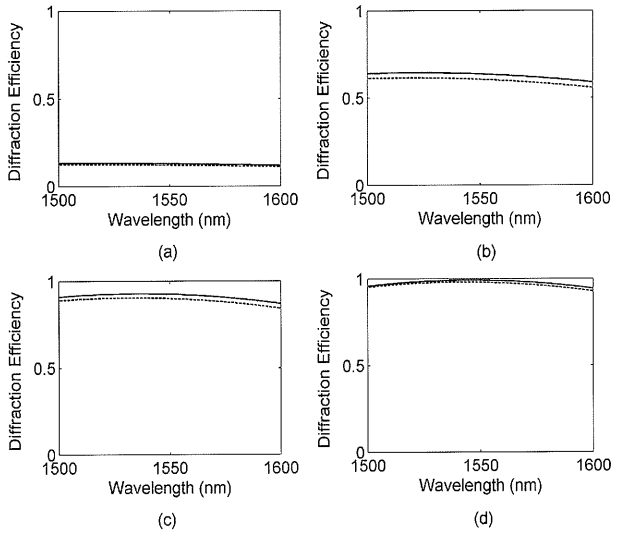

Fig. 3. Calculated diffraction efficiencies as functions of wavelength of volume phase transmission gratings for both TE (solid line) and TM (dotted line) polarizations. (a) $\Delta n = 0.002$; (b) $\Delta n = 0.005$; (c) $\Delta n = 0.007$; (d) $\Delta n = 0.008$. The four gratings have the same parameters of $d = 76\,\mu\mathrm{m}$, $\lambda_0 = 1550\,\mathrm{nm}$, $n = 1.44$ and $\theta_{01} = 25°$, $\theta_{02} = 40°$.

possible with reasonable refractive index modulation Δn as long as d is sufficiently large and $\Delta\theta$ sufficiently small.

3. Compact Configurations

We now consider two possible compact optics configurations for multi/demultiplexers, as shown schematically in Fig. 4. In the first conventional substrate-mode configuration[13] shown in Fig. 4(a), the light is guided inside the substrate by total internal reflection. When the incident angle inside the substrate is $\theta_1 = \theta_{01}$, then the angular dispersion of the first grating at wavelength λ is

$$\frac{d\theta_{02}}{d\lambda} = \frac{\sin(\theta_{02}) - \sin(\theta_{01})}{\lambda_0 \cdot \cos(\theta_2)}, \tag{3}$$

where θ_2 is the diffracted angle inside the substrate at wavelength λ, given by

$$\theta_2 = \sin^{-1}\left[\sin(\theta_{01}) + [\sin(\theta_{02}) - \sin(\theta_{01})] \cdot \frac{\lambda}{\lambda_0}\right]. \tag{4}$$

As evident from Eq. (3), the angular dispersion is small if $\Delta\theta$ is small, i.e. if θ_{02} is close to θ_{01}, which is required in order to relax the polarization dependence and wavelength discrimination of the grating.

In the second new compact configuration shown in Fig. 4(b), the diffracted beams propagate in the air cavity between the two substrates, rather than through the substrate. The internal surfaces of the substrates are coated with reflective layers, so that the propagating beams can be totally reflected and guided in the air from one grating to the other. In this configuration, the angular dispersion of the first grating at wavelength λ is

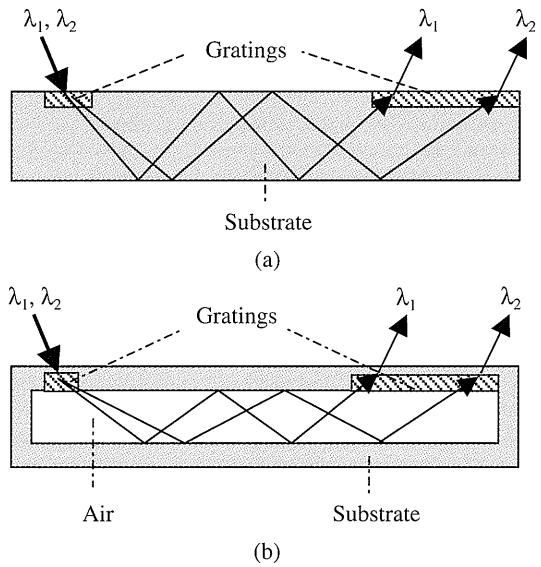

Fig. 4. Two compact configurations for CWDM and CWDDM. (a) Conventional substrate-mode configuration where light is guided inside the substrate by total internal reflection; (b) new compact configuration where light is guided in air between two parallel substrates whose internal surfaces are coated with reflective layers.

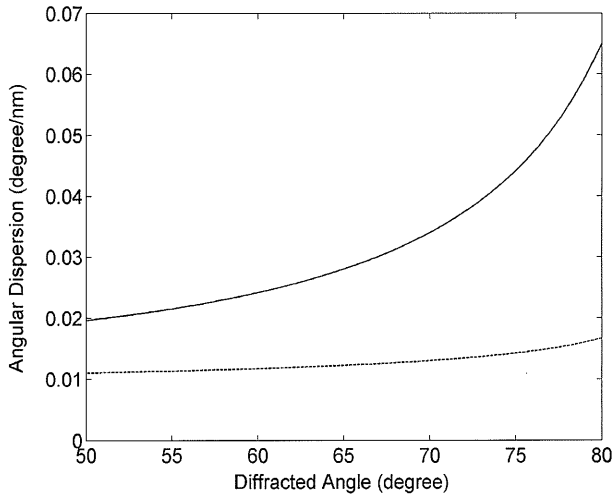

Fig. 5. Calculated angular dispersions as functions of diffracted angle for the conventional configuration shown in Fig. 4(a) (dotted line), and for the new configuration shown in Fig. 4(b) (solid line). The related parameters are $\lambda_0 = 1550\,\text{nm}$, $n = 1.44$ and $\theta_{02} - \theta_{01} = 15°$.

$$\frac{d\theta_2^{\text{air}}}{d\lambda} = \frac{\sin(\theta_{02}) - \sin(\theta_{01})}{\lambda_0} \cdot \frac{n}{\sqrt{1 - n^2\sin^2(\theta_2)}}, \tag{5}$$

where θ_2^{air} is the diffracted angle in the air and refracted from the substrate at wavelength λ, and θ_2 must fulfil the condition $\theta_2 < \arcsin(1/n)$ in order to ensure that light would be refracted from the substrate into the air.

By comparing Eqs. (3) and (5), it is clear that the angular dispersion in the new compact configuration is significantly higher than in the conventional substrate-mode configuration. Figure 5 shows the calculated results of angular dispersion as functions of diffracted angle for both compact configurations. For these calculations, $\lambda_0 = 1550\,\text{nm}$, $n = 1.44$, and $\theta_{02} - \theta_{01} = 15°$. As expected, the angular dispersion for the new configuration where the light diffracted from the first grating propagates in air is indeed larger than when it propagates through the substrate. This is particularly evident when the diffracted angle is larger than 65°.

It is true that unlike the substrate-mode configuration where the total internal reflection is practically 100%, there would be some intensity loss in the air cavity configuration at the optical coatings. This loss is particularly troublesome when metallic coatings are used. However, with proper dichroic reflective coatings which cover the entire angular and spectral ranges of the light, very high reflections of 97% and more can be obtained. Thus, the undesired intensity losses will not be significant.

Based on these results and analysis, we concluded that the new configuration in which light propagates in the air, shown in Fig. 4(b), is preferred because of the larger angular dispersion. Moreover, when the diffracted angle θ_{02} increases, then the angular dispersion will be even larger. This improvement in angular dispersion would be even higher if n were increased.

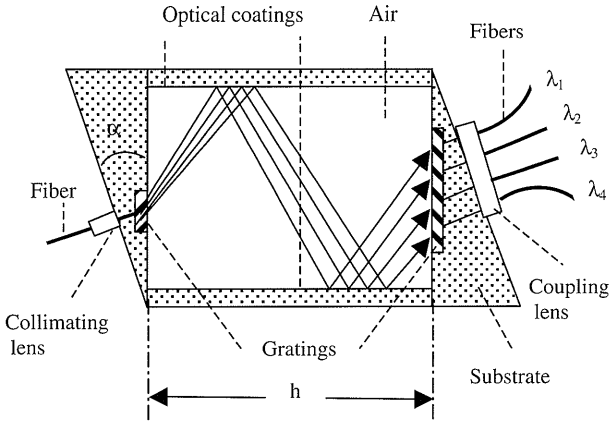

Fig. 6. Compact configuration of a four-channel demultiplexer for CWDDM.

4. Experimental Procedure and Results

We designed and recorded gratings for a four-channel demultiplexer for CWDDM, where the central wavelengths were 1510 nm, 1535 nm, 1560 nm and 1585 nm. The overall configuration, as shown in Fig. 6, is shaped as a parallelogram with an internal air cavity where the light diffracted from one grating propagates to the other. Two parallel and identical volume phase transmission gratings were recorded on either side of the cavity. The tilting angle α was chosen to be equal to the Bragg incident angle at the central wavelength $\lambda_0 = 1550$ nm. This was to ease the alignment, whereby the normally incident input beam automatically fulfils the Bragg condition of the first grating at wavelength λ_0. This was also true for the output beam which emerges normally from the configuration.

Light from a source-input fiber of composite wavelength channels of λ_1, λ_2, λ_3, λ_4, was collimated through a coupling lens to form plane waves that are incident on the first grating with angle α. The first grating acts as a dispersive component, diffracting the four wavelength channels into four diffracted plane waves, each to a different angle in accordance with its wavelength. The four wavelength channels are further angularly separated when the diffracted plane waves are refracted into the air cavity. The upper and lower substrate surfaces inside the cavity were coated with reflective layers, so the four diffracted plane waves from the first grating propagate through the cavity while increasing the spatial separations between them before arriving at the second grating. The second grating redirects all four plane waves so they emerge from the second grating in parallel but spatially separated. Each is then easily coupled into a corresponding fiber with a coupling lens. The spatial channel separations were

$$x_m = h \times \tan(\theta_{m+1}^{\text{air}}) - h \times \tan(\theta_m^{\text{air}}) \tag{6}$$

where h is the length of the cavity, $m = 1, 2, 3$, and

$$\theta_m^{\text{air}} = \sin^{-1}\left[\frac{\sin(\theta_{02}) - \sin(\theta_{01})}{\lambda_0} \cdot \lambda_m \cdot n + \sin(\theta_{01}) \cdot n\right]. \tag{7}$$

The gratings, which were designed to have the calculated diffraction efficiencies as functions of wavelength for both TE and TM polarizations shown in Fig. 3(d), were holographically recorded in photopolymers[14] 76 μm thick with a recording wavelength $\lambda_r = 488$ nm. The two recording angles in the air were calculated to be 47.21° and 56.62°, so that the Bragg incident angle θ_{01} and diffracted angle θ_{02} inside the grating layer were 25° and 40° at the readout wavelength of $\lambda_0 = 1550$ nm. This resulted in $\Delta\theta = 15°$, small enough to have low polarization dependence and negligible wavelength discrimination in the wavelength range of 1500 nm to 1600 nm. Moreover, θ_{02} was 40°, big enough to provide larger angular dispersion, but smaller than the critical angle $\arcsin(1/n) = 44°$, for $n = 1.44$ so that the diffracted light from the first grating could be refracted from the substrate into the air cavity. The recording exposure was adjusted during the experiments to approach the optimum refractive index modulation, approximately $\Delta n = 0.008$, for the maximum diffraction efficiency.

We measured the diffraction efficiency of the first grating as a function of wavelength using a tunable diode laser with a spectral tuning range from 1505 nm to 1590 nm. The measurements were performed for both TE and TM polarizations. The experimental results are presented in Fig. 7, along with the fitting curves. As predicted, this grating indeed has a high and relatively uniform diffraction efficiency as a function of wavelength over the entire wavelength range from 1505 nm to 1590 nm with little polarization dependence. To determine the average angular dispersion of the first grating, we used the following definition,

$$\left.\frac{d\theta_2^{\text{air}}}{d\lambda}\right|_{\text{ave}} = \frac{\theta_{22}^{\text{air}} - \theta_{21}^{\text{air}}}{\lambda_2 - \lambda_1}, \tag{8}$$

where θ_{22}^{air} and θ_{21}^{air} are the diffracted angles in the air for λ_2 and λ_1 respectively. Using $\lambda_2 = 1590$ nm and $\lambda_1 = 1505$ nm, we measured the corresponding diffracted angles θ_{22}^{air} and θ_{21}^{air}, and calculated the average angular dispersion in

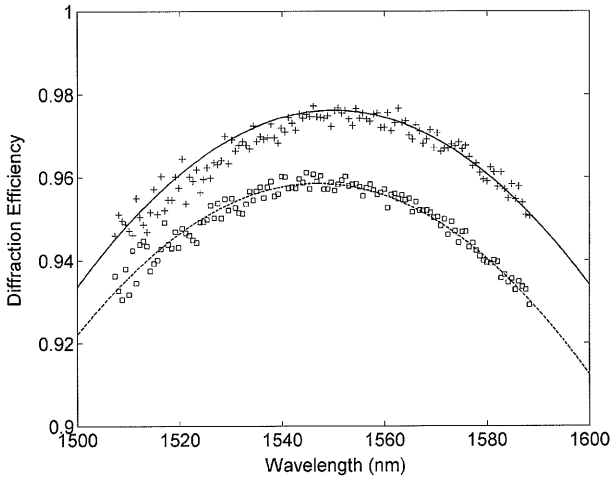

Fig. 7. Experimental results and fitting curves of diffraction efficiency as functions of wavelength for both TE and TM polarizations. Solid line: fitting curve for TE polarization results denoted by +. Dotted line: fitting curve for TM polarization denoted by □.

accordance with Eq. (8). The result was 0.0282°/nm. For comparison, we also calculated the angular dispersion at illumination wavelengh $\lambda_0 = 1550\,\text{nm}$ in accordance with Eq. (5), using the measured grating parameters. The result was 0.0285°/nm, which was in good agreement with the experimental results.

We then determined the lateral displacement of the beams emerging from the entire demultiplexer configuration, where the distance h between the gratings was 30 mm. The input plane wave derived from the tunable diode laser was varied sequentially to specific discrete wavelengths of 1510 nm, 1535 nm, 1560 nm, and 1585 nm. The input plane waves were efficiently diffracted by the first grating, propagated through the air cavity, and finally were redirected by the second grating to form four parallel, laterally displaced output beams. The lateral separations between adjacent beams were measured as 1.69 mm, 1.82 mm and 1.92 mm. These experimental results were in close agreement with the calculated results of 1.68 mm, 1.80 mm and 1.94 mm according to Eqs. (6) and (7) for $\lambda_0 = 1550\,\text{nm}$, $h = 30\,\text{mm}$, $n = 1.401$. Such separations are sufficient for each wavelength channel to be easily detected independently with little, if any, crosstalk. For comparison, the lateral separations between adjacent beams in the substrate mode configuration estimated under the same device-size condition were 0.23 mm, 0.24 mm, and 0.24 mm.

5. Concluding Remarks

Volume phase transmission gratings were designed, recorded and experimentally evaluated to have high and uniform diffraction efficiency with negligible polarization dependence in a broad wavelength range from 1500 nm to 1600 nm. A relatively large angular wavelength dispersion can be obtained when the gratings are incorporated into a novel compact configuration where light is guided in the air cavity, instead of the substrate. A four-channel demultiplexer for CWDDM was designed and constructed to operate at a central wavelength of 1550 nm. The experimental results with this demultiplexer clearly demonstrate that this compact configuration is indeed suitable for CWDM and CWDDM applications.

Acknowledgements

This research was supported in part by Pamot Venture Capital Fund through Plan-Op Ltd. The authors would like to thank Dr. Revital Shechter for helpful discussions.

References

1) L. Kazovsky: *Optical Fiber Communication Systems*, eds. S. Benedetto and A. Willner (Artech House, Boston, London, 1996) Chap. 7.
2) G. E. Keiser: Opt. Fiber Technol. **5** (1999) 3.
3) J. J. Petiote: WDM Solutions (Jan, 2001) 47.
4) J. Minowo and Y. Fuji: J. Lightwave Technol. **1** (1983) 116.
5) Y. T. Huang, D. C. Su and Y. K. Tsai: Opt. Lett. **17** (1992) 629.
6) M. M. Li and R. T. Chen: Opt. Lett. **20** (1995) 797.
7) J. Qiao, F. Zhao, J. Liu and R. T. Chen: IEEE Photonics Technol. Lett. **12** (2000) 1070.
8) H. Kogelnik: Bell Syst. Tech. J. **48** (1969) 2909.
9) J. Solymar: *Volume Holography and Volume Gratings*, ed. D. J. Cooke (Academic Press, London, 1981) Chap. 4.
10) J. W. Goodman: *Introduction to Fourier Optics* (McGraw-Hill, New York, 1996) Chap. 9.
11) B. M. Monroe, W. K. Smothers, D. K. Keys, R. R. Krebs, D. J. Mickish, A. F. Harrington, S. R. Schicker, M. K. Armstrong, D. M. T. Chan and C. I. Weathers: J. Imaging Sci. **35** (1991) 19.
12) W. B. Jones: *Introduction to Optical Fiber Communication Systems* (Oxford University Press, New York, 1988) p. 55.
13) A. A. Friesem and Y. Amitai: Trend in Optics (1996) 125.
14) W. K. Smothers, B. M. Monroe, A. M. Weber and D. E. Keys: *Practical Holography IV*, ed. S. A. Benton, Proc. SPIE **1212** (1990) 20.